

Modal-interaction approach to the strong structural–acoustic coupling of an elastic Helmholtz resonator and an acoustic cavity containing a heavy fluid

Miša Oblak^a, Miha Pirnat^a, Miha Boltežar^{b,*}

^a*Kolektor Etra d.o.o., Šlandrova 10, 1231 Ljubljana, Slovenia*

^b*Faculty of Mechanical Engineering, Aškerčeva 6, 1000 Ljubljana, Slovenia*

Cite as:

*Miša Oblak, Miha Pirnat, Miha Boltežar,
Modal-interaction approach to the strong structural–acoustic coupling of an elastic
Helmholtz resonator and an acoustic cavity containing a heavy fluid,
Journal of Sound and Vibration 535 (2022) 117120,
<https://doi.org/10.1016/j.jsv.2022.117120>*

Abstract

This paper focuses on the development of a method for the accurate representation of the strong structural–acoustic coupling between an elastic Helmholtz resonator, a heavy fluid and an impedance tube. The Helmholtz resonator has an elastic wall and is connected to the impedance tube, yielding a system with two acoustic cavities coupled through a neck and the fluid–structure interaction between a liquid medium and a plate. The proposed analytical formulation is based on the modal superposition method in combination with a lumped parameter model of the neck. The effect of the evanescent waves is taken into account in the form of both the inertial attached length of the neck and the terms of the evanescent pressure modes in the governing equations, which are omitted in other methods. The formulation of the evanescent pressure field is redefined to include the reflected waves, thus expanding the application to the acoustic cavity of an arbitrary shape. Strong coupling between the heavy fluid and the plate is accomplished with the implementation of the non-resonant acoustic modes. Furthermore, the improved performance of the model for moderately thick plates is achieved with the combined approach of the Mindlin–Reissner theory mode shapes and the Kirchhoff–Love theory governing equations. The proposed model is validated with FEA simulations of three different resonator configurations and compared to other applicable methods. The results demonstrate substantially increased accuracy in the predicted response of the coupled structural–acoustic system.

*Corresponding author. Tel.: +386 1 4771 608

Email addresses: misa.oblak@kolektor.com (Miša Oblak), miha.pirnat@kolektor.com (Miha Pirnat), miha.boltezar@fs.uni-lj.si (Miha Boltežar)

Keywords: modal-interaction, fluid-structure interaction, structural–acoustic coupling, Mindlin plate, Kirchhoff plate, heavy fluid, Helmholtz resonator, impedance tube

1. Introduction

The Helmholtz resonator has been extensively researched for the purpose of low-frequency sound absorption in airborne applications [1]. Its implementation in heavy fluids is a greater challenge due to the longer wavelengths and corresponding dimensional constraints. Generally, a resonator with elastic walls has a lower resonance frequency than an acoustically rigid resonator [2, 3], which suggests the potential for low-frequency performance in liquids comparable to a resonator in the air. However, an analytical model is required for a deeper understanding of the underlying physical mechanisms. Furthermore, in practice, Helmholtz resonators are implemented in an acoustic cavity with its own intrinsic dynamic characteristics. The coupling of the internal and external pressure fields can have a significant effect on the resonator’s performance, especially if it involves the strong coupling of a heavy fluid and a structure. Existing studies are often narrowly focused on the individual segments of the presented problem, as summarized in the literature review below. Among these segments is an elastic Helmholtz resonator, coupling of an acoustic cavity and a plate, acoustic cavities connected through an opening and an acoustically rigid Helmholtz resonator coupled to a cavity. Moreover, a strong fluid-structure coupling has been researched. On the other hand, a combined approach to the analysis of a strong structural–acoustic coupling between an elastic Helmholtz resonator, an acoustic cavity and a heavy fluid has not yet been investigated.

Research of the elastic Helmholtz resonator has been in the direction of a resonator with an attached elastic plate or membrane, but otherwise acoustically rigid walls, as a sound absorber for airborne applications. In the literature, an elastic resonator in the air is frequently represented with a simplified lumped-parameter model [4–7], where both the acoustic fluid and the structural membrane are modeled with a spring–mass–damper system, although discrepancies between the calculated and the measured response were reported [6]. Such an approach was also unsuccessfully implemented by Wang *et al.* [8] in a study of a fully elastic, underwater Helmholtz resonator. Hu *et al.* [9] showed that a multi-mode analysis must be implemented in order to accurately predict the performance of an elastic resonator in the relevant frequency range.

The more conventional approach of a modal superposition method [10] is often used for analytical formulations of the problems with coupling between the structures and the enclosed volumes of fluid. An early investigation of the plate-cavity system with modal coupling was conducted by Fahy [11, 12] and further applications of the plate-cavity interaction were researched in [13–15]. Dowell *et al.* [16] presented a general theory of the modal-interaction approach and extended the use to multiple cavities connected through with apertures. Lee *et al.* [17, 18] proposed an alternative formulation for the cavities connected

by a neck or an opening of small size compared to the wavelength. Representing the cavities' pressure field as a sum of standing waves and evanescent waves, a more accurate pressure field at the geometric discontinuity was achieved with fewer degrees of freedom. The neck was modeled as a lumped mass and the inertial attached length of the neck was taken into account. Evanescent waves were used to determine the inertial attached neck length, but were omitted in the governing equations for the coupled system. A similar approach of the lumped neck was employed in the research of cavities coupled through a plate with holes [19] and a fully elastic silicone Helmholtz resonator [20], although the evanescent waves were not considered and the inertial attached neck length was taken from the literature [21].

In the field of an acoustically rigid resonator coupled to an air-filled enclosure, an early modal-interaction model with the interaction between a lumped-parameter resonator and a single cavity mode was proposed by Fahy and Schofield [22]. Related approaches later extended the model to include an array of resonators [23], multiple cavity modes [24] and an open cavity [25], while preserving the simplified representation of the resonator with a lumped-parameter model. An adaptive resonator with an internal flexible plate for the sound attenuation in a small enclosure was designed by Cui and Harne [26]. With the equivalent lumped parameter system the model was again limited to the coupling of a single cavity and the resonator mode. Otherwise, reports of research in the field of the elastic resonator coupled with a cavity are sparse.

The outlined research was predominantly performed using air-filled cavities and Helmholtz resonators. Often in the case of a light fluid, a considerable impedance mismatch between the elastic structure and the acoustic volume is present, resulting in weak coupling. In contrast, liquids are dense and less compressible fluids with a substantial influence on the structural stiffness and mass, producing a strong fluid-structure coupling. Kim and Brennan [27] validated the modal-interaction approach on both weakly and strongly coupled cavity-plate systems, although both experiments were conducted in the air. The interaction between a plate and a water-filled cavity was researched by David *et al.* [28, 29] and Maxit [30]. In addition to the typical interaction between the acoustic and structural modes in the excited frequency range in the case of a light fluid, the authors observed a significant contribution from the cavity modes with a much higher natural frequency.

Considering the lack of research on the interconnected coupling of the elastic Helmholtz resonator, a heavy fluid and an acoustic cavity, the aim of this paper is to develop an analytical model for the analysis of such a structural-acoustic system. The model should predict the response of the coupled system in a wider frequency range around the natural frequency of the elastic Helmholtz resonator. While comparable formulations were presented by Lee *et al.* [18] and Cui *et al.*[20], their models do not provide enough accuracy due to an insufficient consideration of the evanescent waves. Based on that, new governing equations of the modal-interaction approach are derived to include terms for the evanescent pressure-field modes. The corresponding evanescent wave for-

mulation is expanded to accommodate reflections in the cavity of an arbitrary size. Furthermore, the combination of the Kirchhoff-Love plate theory and the Mindlin–Reissner plate theory is proposed to improve the performance of the model for moderately thick plates. The developed model is validated with the harmonic finite-element analysis (FEA) of a coupled system with a heavy fluid. The scope of the work also includes a comprehensive study of the influence of the evanescent waves on the accuracy, and a comparison between the proposed model and other applicable approaches [18, 20].

To begin with, the theoretical foundations of the plate vibration and the acoustic waves’ propagation are presented in Section 2. The modal-interaction approach is applied to derive the governing equations of the system dynamics, taking into account the exponentially decaying evanescent waves. Furthermore, the formulation of the evanescent pressure field is expanded to include the reflected waves in short cavities and the inertial attached length of the neck is expressed in the form of an evanescent-wave pressure. Explicit terms of the governing equations for cylindrical cavities and circular plate are presented in Appendix A. The proposed model is validated with a FEA model of three different configurations of the elastic Helmholtz resonator coupled to the impedance tube in Section 3. Based on the observed discrepancies for the resonators with thick plates, the combined approach of using the Kirchhoff-Love and the Mindlin–Reissner plate theory is established. The advantages of the current model in comparison to the other modal-interaction methods are discussed and the effects of evanescent waves on the pressure distribution are analyzed.

2. Analytical formulation

The subject of the study is a partially elastic Helmholtz resonator coupled to an impedance tube, as shown in Fig. 1. The impedance tube and the resonator are filled with a heavy fluid (liquid) and have acoustically rigid walls, except for the elastic plate on the bottom of the resonator. The modal-interaction formulation is used to develop an analytical model for the coupling between multiple cavities and the plate. With this approach, the internal pressure field and the structure displacement are expressed with the superposition of the uncoupled mode shapes and the coupled modal coordinates.

2.1. Equation of elastic plate

Observing the transverse vibration of a thin Kirchhoff plate, the plate displacement $w(\mathbf{r}_P, t)$ at the location \mathbf{r}_P and time t is governed by the following differential equation [10]:

$$D \nabla^4 w(\mathbf{r}_P, t) + \rho_P h \frac{\partial^2 w(\mathbf{r}_P, t)}{\partial t^2} = p(\mathbf{r}_P, t) + f(\mathbf{r}_P, t), \quad (1)$$

where the plate density ρ_P and thickness h together form the area density. The potential excitation sources are expressed with $p(\mathbf{r}_P, t)$ as an acoustic pressure

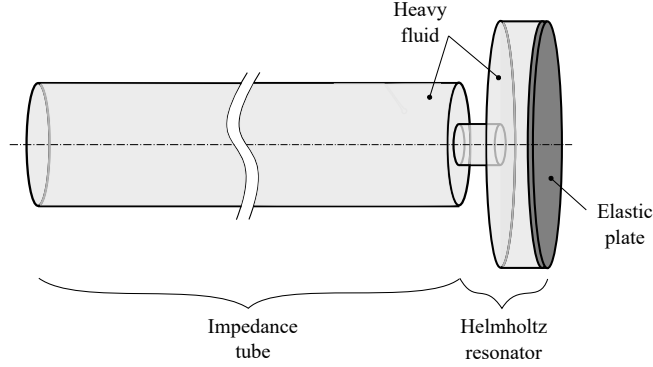


Figure 1: Coupled structural–acoustic system with an impedance tube and a Helmholtz resonator having an elastic plate.

loading and $f(\mathbf{r}_P, t)$ as an externally applied force. The flexural stiffness D is characterized by the Young’s modulus E and the Poisson’s ratio ν :

$$D = \frac{E h^3}{12(1 - \nu^2)}. \quad (2)$$

Following the superposition principle, the plate’s response can be defined as the sum of the *in vacuo* mode shapes $\phi_p(\mathbf{r}_P)$ times the modal displacement amplitudes $w_p(t)$:

$$w(\mathbf{r}_P, t) = \sum_p w_p(t) \phi_p(\mathbf{r}_P) = \sum_p \bar{w}_p \phi_p(\mathbf{r}_P) e^{j\omega t}, \quad (3)$$

when assuming a harmonic excitation and response. *In vacuo* mode shapes $\phi_p(\mathbf{r}_P)$ are orthogonal with respect to the plate’s surface S_P :

$$\int_{S_P} \phi_{p_i}(\mathbf{r}_P) \phi_{p_j}(\mathbf{r}_P) dS_P = \begin{cases} 0 & p_i \neq p_j \\ \mu_p & p_i = p_j = p \end{cases}, \quad (4)$$

and satisfy the homogeneous differential equation:

$$D \nabla^4 \phi_p(\mathbf{r}_P) - \rho_P h \omega_p^2 \phi_p(\mathbf{r}_P) = 0. \quad (5)$$

2.2. Equation of acoustic cavities

On the other hand, the propagation of the acoustic waves is governed by the acoustic wave equation [10]:

$$\nabla^2 p(\mathbf{r}, t) - \frac{1}{c^2} \frac{\partial^2 p(\mathbf{r}, t)}{\partial t^2} = -\rho \frac{\partial q(\mathbf{r}, t)}{\partial t}, \quad (6)$$

where the position vector \mathbf{r} refers to a point in the fluid volume, c is the sound speed, ρ is the fluid density and $q(\mathbf{r}, t)$ represents the volume velocity per unit

volume of the excitation source. The acoustic pressure $p(\mathbf{r}, t)$ in the cavities connected through the necks or apertures can be divided into the standing-waves pressure $p_A(\mathbf{r}, t)$ and evanescent-waves pressure $p_E(\mathbf{r}, t)$ [17, 18]:

$$p(\mathbf{r}, t) = p_A(\mathbf{r}, t) + p_E(\mathbf{r}, t). \quad (7)$$

The pressure $p_A(\mathbf{r}, t)$ corresponds to the propagating waves with a real-value wavenumber and the pressure $p_E(\mathbf{r}, t)$ corresponds to the exponentially decaying waves with an imaginary-value wavenumber. Under the assumption of a harmonic response we can write each pressure field inside the acoustic cavity as:

$$p_A(\mathbf{r}, t) = \sum_a p_a(t) \psi_a(\mathbf{r}) = \sum_a \bar{p}_a \psi_a(\mathbf{r}) e^{j\omega t}, \quad (8)$$

$$p_E(\mathbf{r}, t) = \sum_e p_e(t) \psi_e(\mathbf{r}) = \sum_e \bar{p}_e \psi_e(\mathbf{r}) e^{j\omega t}, \quad (9)$$

where $p_{a,e}(t)$ is the modal pressure amplitude and $\psi_{a,e}(\mathbf{r})$ is the rigid-wall cavity mode shape, with indices a and e denoting the mode order of the standing and the evanescent waves, respectively. Again, the acoustic mode shapes are orthogonal and can be obtained with the homogeneous differential equations:

$$\nabla^2 \psi_a(\mathbf{r}) + k_a^2 \psi_a(\mathbf{r}) = 0, \quad (10)$$

$$\nabla^2 \psi_e(\mathbf{r}) + k^2 \psi_e(\mathbf{r}) = 0, \quad (11)$$

$$\int_V \psi_{a_i}(\mathbf{r}) \psi_{a_j}(\mathbf{r}) dV = \begin{cases} 0 & a_i \neq a_j \\ \mu_a & a_i = a_j = a \end{cases}, \quad (12)$$

$$\int_V \psi_{e_i}(\mathbf{r}) \psi_{e_j}(\mathbf{r}) dV = \begin{cases} 0 & e_i \neq e_j \\ \mu_e & e_i = e_j = e \end{cases}, \quad (13)$$

where $k_a = \frac{\omega_a}{c}$ relates to the wavenumber at the natural angular frequency ω_a . In contrast, the evanescent waves are propagating with the response frequency ω , explaining the use of the corresponding wavenumber $k = \frac{\omega}{c}$ in Eq. (11). Cavity mode shape $\psi_a(\mathbf{r})$ with natural frequency $\omega_a = 0$ represents the static pressure term, which accounts for the zero-frequency influence on the structural stiffness and mass.

2.3. Modal-interaction model

The coupled system in Fig.1 is divided into two acoustic cavities and a structural plate with known uncoupled mode shapes, as shown in Fig. 2, in order to develop the analytical formulation using the modal-interaction approach. Cavity 1 and cavity 2 represent the resonator cavity and the impedance tube. The plate and each cavity comply with the corresponding wave equations (Eq. (1) and (6)). Cavity 1 is coupled to the plate, which introduces the additional excitation source $-\rho \frac{\partial q(\mathbf{r}, t)}{\partial t}$ of Eq. (6), representing the normal plate vibration:

$$q_P(\mathbf{r}, t) = -2 \frac{\partial w(\mathbf{r}_P, t)}{\partial t} \delta(z - z_P), \quad (14)$$

while assuming that the plate's displacement is directed outwards from the fluid volume. The Dirac delta function $\delta(z - z_P)$ limits the volume velocity $q_P(\mathbf{r}, t)$ to the infinitesimal interface layer under the plate at the location $z_P = L_2 + L_N + L_1$.

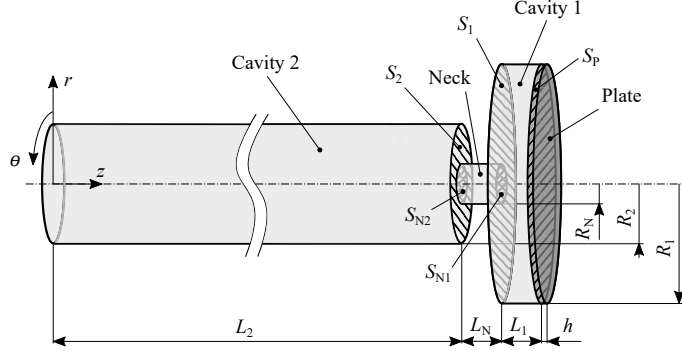


Figure 2: Cylindrical system with two acoustic cavities coupled through a neck and the fluid-structure interaction between a cavity and a plate.

The two cavities in Fig. 2 are coupled through the neck. Under the assumption of small dimensions in comparison to the wavelength, the neck can be modeled as a lumped mass with the displacement $\xi_N(t)$. Formulating the lumped-mass vibration equivalently to the plate's excitation in Eq. (14) and limiting the volume flow $q(\mathbf{r}, t)$ to the location of the source \mathbf{r}_q , problem-specific wave equations are obtained for cavities 1 and 2:

$$\nabla^2 p_1(\mathbf{r}, t) - \frac{1}{c^2} \frac{\partial^2 p_1(\mathbf{r}, t)}{\partial t^2} = 2\rho \frac{\partial^2 w(\mathbf{r}_P, t)}{\partial t^2} \delta(z - z_P) - 2\rho \ddot{\xi}_N(t) \delta(z - z_1) - \rho \frac{\partial q_1(\mathbf{r}, t)}{\partial t} \delta(\mathbf{r} - \mathbf{r}_{q_1}), \quad (15)$$

$$\nabla^2 p_2(\mathbf{r}, t) - \frac{1}{c^2} \frac{\partial^2 p_2(\mathbf{r}, t)}{\partial t^2} = 2\rho \ddot{\xi}_N(t) \delta(z - z_2) - \rho \frac{\partial q_2(\mathbf{r}, t)}{\partial t} \delta(\mathbf{r} - \mathbf{r}_{q_2}), \quad (16)$$

where $z_1 = L_2 + L_N$ refers to the location of the interface between the neck and cavity 1; the same applies to the interface between the neck and cavity 2 with $z_2 = L_2$. Replacing the acoustic pressure p_1 in Eq. (15) with Eq. (7)-(9) and applying Eq. (10)-(11) results in:

$$\begin{aligned} & - \sum_{a_1} k_{a_1}^2 p_{a_1}(t) \psi_{a_1}(\mathbf{r}) - \frac{1}{c^2} \sum_{a_1} \ddot{p}_{a_1}(t) \psi_{a_1}(\mathbf{r}) - \\ & - \sum_{e_1} k^2 p_{e_1}(t) \psi_{e_1}(\mathbf{r}) - \frac{1}{c^2} \sum_{e_1} \ddot{p}_{e_1}(t) \psi_{e_1}(\mathbf{r}) = \\ & = 2\rho \frac{\partial^2 w(\mathbf{r}_P, t)}{\partial t^2} \delta(z - z_P) - 2\rho \ddot{\xi}_N(t) \delta(z - z_1) - \\ & - \rho \frac{\partial q_1(\mathbf{r}, t)}{\partial t} \delta(\mathbf{r} - \mathbf{r}_{q_1}). \end{aligned} \quad (17)$$

Furthermore, multiplying both sides of the equation with the cavity mode shapes $\psi_{a_1}(\mathbf{r})$, integrating over the cavity-1 volume and taking into account the orthogonality of the mode shapes in the form of Eq. (12) transforms into:

$$\begin{aligned}
& -\mu_{a_1} k_{a_1}^2 p_{a_1}(t) - \frac{1}{c^2} \mu_{a_1} \ddot{p}_{a_1}(t) - \\
& -k^2 \sum_{e_1} p_{e_1}(t) \int_{V_1} \psi_{e_1}(\mathbf{r}) \psi_{a_1}(\mathbf{r}) dV_1 - \\
& -\frac{1}{c^2} \sum_{e_1} \ddot{p}_{e_1}(t) \int_{V_1} \psi_{e_1}(\mathbf{r}) \psi_{a_1}(\mathbf{r}) dV_1 = \\
& = \rho \int_{S_P} \frac{\partial^2 w(\mathbf{r}_P, t)}{\partial t^2} \psi_{a_1}(\mathbf{r}_P) dS_P - \rho \int_{S_{N1}} \ddot{\xi}_N(t) \psi_{a_1}(\mathbf{r}_1) dS_{N1} - \\
& - \rho \int_{V_1} \frac{\partial q_1(\mathbf{r}, t)}{\partial t} \delta(\mathbf{r} - \mathbf{r}_{q_1}) \psi_{a_1}(\mathbf{r}) dV_1, \tag{18}
\end{aligned}$$

with the volume integrals of the structural excitation sources reverting to the surface integrals over the fluid-structure interface S_P for the plate and over the cavity-neck interface S_{N1} for the neck at location \mathbf{r}_1 (Fig. 2). Equivalent to the derivation in [18], we obtained the modal equation for a single standing-wave modal coordinate $p_{a_1}(t)$. At this point the proposed model introduces a crucial improvement. Observing Eq. (18), the modal coordinate $p_{a_1}(t)$ propagates with the natural frequency ω_{a_1} and the corresponding set of evanescent waves should propagate with the same frequency. Therefore, the wavenumber k is replaced with k_{a_1} , yielding:

$$\begin{aligned}
& -\mu_{a_1} k_{a_1}^2 p_{a_1}(t) - \frac{1}{c^2} \mu_{a_1} \ddot{p}_{a_1}(t) - \\
& -k_{a_1}^2 \sum_{e_1} I_{a_1 e_1} p_{e_1}(t) - \frac{1}{c^2} \sum_{e_1} I_{a_1 e_1} \ddot{p}_{e_1}(t) = \\
& = \rho \int_{S_P} \frac{\partial^2 w(\mathbf{r}_P, t)}{\partial t^2} \psi_{a_1}(\mathbf{r}_P) dS_P - \rho \int_{S_{N1}} \ddot{\xi}_N(t) \psi_{a_1}(\mathbf{r}_1) dS_{N1} - \\
& - \rho \int_{V_1} \frac{\partial q_1(\mathbf{r}, t)}{\partial t} \delta(\mathbf{r} - \mathbf{r}_{q_1}) \psi_{a_1}(\mathbf{r}) dV_1, \tag{19}
\end{aligned}$$

where $I_{a_1 e_1}$ represents the dimensionless coupling coefficient given by the integral $\int_{V_1} \psi_{a_1}(\mathbf{r}) \psi_{e_1}(\mathbf{r}) dV_1$. Finally, implementing Eq. (3) and assuming harmonic excitation the following equation is obtained:

$$\begin{aligned}
& \mu_{a_1} (\omega^2 - \omega_{a_1}^2) \bar{p}_{a_1} + (\omega^2 - \omega_{a_1}^2) \sum_{e_1} I_{a_1 e_1} \bar{p}_{e_1} = \\
& = -\omega^2 \rho c^2 \left(\sum_p I_{a_1 p} \bar{w}_p - \bar{\xi}_N I_{a_1 N} - \frac{1}{j\omega} \int_{V_1} \bar{q}_1 \delta(\mathbf{r} - \mathbf{r}_{q_1}) \psi_{a_1}(\mathbf{r}) dV_1 \right), \tag{20}
\end{aligned}$$

with $I_{a_1 N}$ referring to the integral $\int_{S_{N1}} \psi_{a_1}(\mathbf{r}_1) dS_{N1}$. The coupling coefficient $I_{a_1 p} = \int_{S_P} \psi_{a_1}(\mathbf{r}_P) \phi_p(\mathbf{r}_P) dS_P$ indicates the coupling strength between the

acoustic mode shape $\psi_{a_1}(\mathbf{r}_P)$ and the structural mode shape $\phi_p(\mathbf{r}_P)$. The parameters $\bar{\xi}_N$ and \bar{q}_1 represent the amplitude of the neck lumped-mass displacement and the amplitude of the volumetric excitation source. We can observe how Eq. (20) differs from the approach of Lee *et al.* [18], where the propagating frequency of the evanescent mode is assumed to be equal to the excitation frequency, which results in an abbreviation of the term $(\omega^2 - \omega_{a_1}^2) \sum_{e_1} I_{a_1 e_1} \bar{p}_{e_1}$. Consequently, a significant effect of the evanescent waves is omitted.

2.4. Evanescent waves

Evanescent waves are developed at a geometric discontinuity, i.e., an aperture or a neck, when the wave propagates from a smaller to a larger cross-section. They are composed of the pressure cross-modes and decay exponentially. Lee *et al.* [17, 18] proposed a formulation for the evanescent pressure field with a set of pressure cross-modes $\phi_{n_i s_i}(\mathbf{r}_i)$, transforming Eq. (9) into:

$$\bar{p}_{E_1}(\mathbf{r}) = \sum_{e_1} \bar{p}_{e_1} \psi_{e_1}(\mathbf{r}) = \sum_{n_1} \sum_{s_1} \bar{p}_{n_1 s_1} \phi_{n_1 s_1}(r, \theta) e^{-\alpha_{n_1 s_1} (z - z_1)} \quad (21)$$

$$\bar{p}_{E_2}(\mathbf{r}) = \sum_{e_2} \bar{p}_{e_2} \psi_{e_2}(\mathbf{r}) = \sum_{n_2} \sum_{s_2} \bar{p}_{n_2 s_2} \phi_{n_2 s_2}(r, \theta) e^{\alpha_{n_2 s_2} (z - z_2)}, \quad (22)$$

where the indices n_i and s_i are not zero at the same time, thus excluding the zero-frequency cross-mode with both a radial and a circumferential order equal to zero. The location z_i marks the contact area between the neck and the corresponding cavity. The pressure cross-modes are assumed to have the same shape as the standing-wave modes in the cavity. In a cylindrical cavity the cross-modes are expressed in the following form:

$$\phi_{n_i s_i}(r, \theta) = J_{n_i} \left(\beta_{n_i s_i} \frac{r}{R_i} \right) \cos(n_i \theta), \quad (23)$$

and the decay rate $\alpha_{n_i s_i}$ is defined as:

$$\alpha_{n_i s_i} = \sqrt{\left(\frac{\beta_{n_i s_i}}{R_i} \right)^2 - k^2}, \quad (24)$$

where the coefficients $\beta_{n_i s_i}$ are determined with the cavity shape and present the roots of the following equation with the derivative of a Bessel function of the first kind and order n_i :

$$J'_{n_i}(\beta_{n_i s_i}) = 0. \quad (25)$$

The modal pressure amplitude $\bar{p}_{n_i s_i}$ is conditioned by the velocity continuity [18]:

$$\bar{p}_{n_i s_i} = (-1)^i \frac{\rho \omega^2 \bar{\xi}_N \int_{S_{N_i}} \psi_{e_i}(\mathbf{r}_i) dS_{N_i}}{\alpha_{n_i s_i} \int_{S_i} [\psi_{e_i}(\mathbf{r}_i)]^2 dS_i} \quad (26)$$

with the position vector \mathbf{r}_i pointing to the surface S_i at $z = z_i$. Eq. (21)-(22) are appropriate for the cases where length of the cavity i complies with the condition $e^{-\alpha_{n_i s_i} L_i} \approx 0$ so as to ensure the total decay of the evanescent wave before reaching the cavity termination. In contrast, the cavity of the Helmholtz resonator in Fig. 2 is short in comparison with the diameter. The propagation of the evanescent waves through the cavities is presented in Fig. 3. Exponential functions in Eq. (21)-(22) would correctly predict the evanescent wave's amplitude in cavity 2 and underestimate the amplitude in cavity 1, where the contribution of the reflected waves would be neglected.

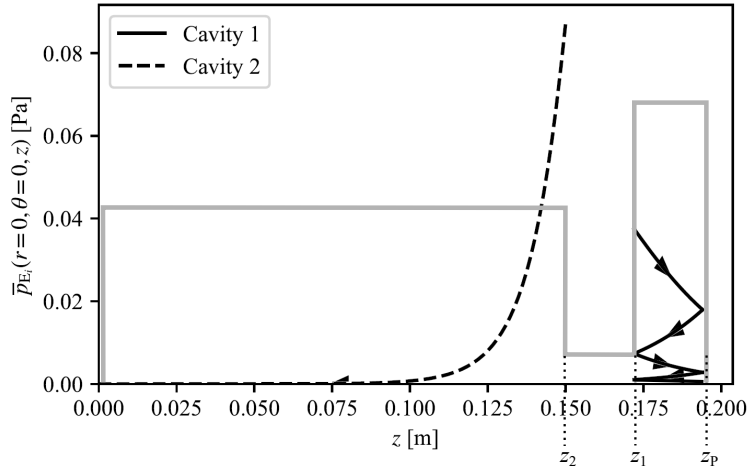


Figure 3: Amplitude of the decaying evanescent waves along the axis z with reflections in cavity 1 and without reflections in cavity 2. Arrows indicate the direction of propagation. Gray outline shows the geometry of the cavities.

In this paper the formulation in Eq. (21)-(22) is expanded to include the reflected evanescent waves:

$$\bar{p}_{E_1}(\mathbf{r}) = \sum_{n_1} \sum_{s_1} \bar{p}_{n_1 s_1} \phi_{n_1 s_1}(r, \phi) C_{n_1 s_1}(z) \quad (27)$$

$$\bar{p}_{E_2}(\mathbf{r}) = \sum_{n_2} \sum_{s_2} \bar{p}_{n_2 s_2} \phi_{n_2 s_2}(r, \phi) C_{n_2 s_2}(z), \quad (28)$$

$$C_{n_1 s_1}(z) = \sum_{m_1} \left\{ e^{-\alpha_{n_1 s_1} [z - (2m_1 - 1)z_1 + (2m_1 - 2)z_P]} + e^{\alpha_{n_1 s_1} [z + (2m_1 - 1)z_1 - 2m_1 z_P]} \right\}, \quad (29)$$

$$C_{n_2 s_2}(z) = \sum_{m_2} \left\{ e^{\alpha_{n_2 s_2} [z - (2m_2 - 1)z_2]} + e^{-\alpha_{n_2 s_2} [z + (2m_2 - 1)z_2]} \right\}. \quad (30)$$

The modal pressure amplitude $\bar{p}_{n_i s_i}$ can then be defined as:

$$\bar{p}_{n_i s_i} = (-1)^i \frac{\rho \omega^2 \bar{\xi}_N \int_{S_{N_i}} \phi_{n_i s_i}(r, \theta) C_{n_i s_i}(z_i) dS_{N_i}}{\alpha_{n_i s_i} \int_{S_i} [\phi_{n_i s_i}(r, \theta) C_{n_i s_i}(z_i)]^2 dS_i}. \quad (31)$$

Considering Eq. (31) it is practical to evaluate the decaying pressure amplitudes $C_{n_1 s_1}(z)$ and $C_{n_2 s_2}(z)$ at the interface of the neck and the cavity \mathbf{r}_i , thus reducing Eq. (29)-(30) to:

$$C_{n_1 s_1}(z_1) = \frac{1 - e^{-2\alpha_{n_1 s_1} L_1 M_1}}{\tanh(\alpha_{n_1 s_1} L_1)}, \quad (32)$$

$$C_{n_2 s_2}(z_2) = \frac{1 - e^{-2\alpha_{n_2 s_2} L_2 M_2}}{\tanh(\alpha_{n_2 s_2} L_2)}, \quad (33)$$

where M_i represents the number of significant pairs of incident and reflected waves, L_2 is the length of the impedance tube (cavity 2) and L_1 is length of the resonator cavity (cavity 1).

2.5. Effective neck length

The evanescent waves increase the apparent length of the neck due to the inertial effect of the fluid motion in close vicinity to the neck inlet and outlet. Displacement of the lumped mass inside the neck is expressed with the following equation of motion [17, 18]:

$$\rho L_N S_N \ddot{\xi}_N(t) = \int_{S_{N2}} p_2(\mathbf{r}_2) dS_{N2} - \int_{S_{N1}} p_1(\mathbf{r}_1) dS_{N1}, \quad (34)$$

where L_N and S_N refer to the geometric neck length and the cross-sectional area, respectively. Employing Eq. (7)-(9) and assuming harmonic motion $\xi_N(t) = \bar{\xi}_N e^{j\omega t}$ we obtain:

$$\rho S_N \omega^2 \bar{\xi}_N L'_N = \sum_{a_1} \bar{p}_{a_1} \int_{S_{N1}} \psi_{a_1}(\mathbf{r}_1) dS_{N1} - \sum_{a_2} \bar{p}_{a_2} \int_{S_{N2}} \psi_{a_2}(\mathbf{r}_2) dS_{N2}, \quad (35)$$

with an effective length of the neck L'_N representing the sum of the geometric length and the inertial attached lengths ΔL_i in each cavity:

$$L'_N = L_N + \Delta L_1 + \Delta L_2 = L_N + \Delta L, \quad (36)$$

$$\Delta L_i = \frac{(-1)^i}{\rho S_N \omega^2 \bar{\xi}_N} \int_{S_{Ni}} \bar{p}_{E_i}(\mathbf{r}_i) dS_{Ni}. \quad (37)$$

2.6. Governing equations

Rearranging Eq. (35) to express the neck displacement:

$$\bar{\xi}_N = \frac{1}{\rho S_N \omega^2 L'_N} \left(\sum_{a_1} \bar{p}_{a_1} I_{a_1 N} - \sum_{a_2} \bar{p}_{a_2} I_{a_2 N} \right), \quad (38)$$

and inserting it into Eq. (20) yields the final form of the governing equation for cavity 1:

$$\mu_{a_1} (\omega^2 - \omega_{a_1}^2) \bar{p}_{a_1} + (\omega^2 - \omega_{a_1}^2) \sum_{e_1} I_{a_1 e_1} \bar{p}_{e_1} -$$

$$\begin{aligned}
& -\frac{c^2}{S_N L'_N} I_{a_1 N} \left(\sum_{a_1} I_{a_1 N} \bar{p}_{a_1} - \sum_{a_2} I_{a_2 N} \bar{p}_{a_2} \right) + \omega^2 \rho c^2 \sum_p I_{a_1 p} \bar{w}_p = \\
& = -j \omega \rho c^2 \int_{V_1} \bar{q}_1 \delta(\mathbf{r} - \mathbf{r}_{q_1}) \psi_{a_1}(\mathbf{r}) dV_1. \tag{39}
\end{aligned}$$

Analogous procedures can be used to derive the equations for cavity 2 and the plate, completing the system of governing equations:

$$\begin{aligned}
& \mu_{a_2} (\omega^2 - \omega_{a_2}^2) \bar{p}_{a_2} + (\omega^2 - \omega_{a_2}^2) \sum_{e_2} I_{a_2 e_2} \bar{p}_{e_2} + \\
& + \frac{c^2}{S_N L'_N} I_{a_2 N} \left(\sum_{a_1} I_{a_1 N} \bar{p}_{a_1} - \sum_{a_2} I_{a_2 N} \bar{p}_{a_2} \right) = \\
& = -j \omega \rho c^2 \int_{V_2} \bar{q}_2 \delta(\mathbf{r} - \mathbf{r}_{q_2}) \psi_{a_2}(\mathbf{r}) dV_2, \tag{40}
\end{aligned}$$

$$\rho_P h \mu_p (\omega^2 - \omega_p^2) \bar{w}_p + \sum_p I_{a_1 p} \bar{p}_{a_1} + \sum_p I_{e_1 p} \bar{p}_{e_1} = - \int_{S_P} \bar{f} \phi_p(\mathbf{r}_P) dS_P. \tag{41}$$

with the following integral representations:

$$\mu_p = \int_{S_P} \phi_p^2(\mathbf{r}_P) dS_P, \tag{42}$$

$$\mu_{a_i} = \int_V \psi_{a_i}^2(\mathbf{r}) dV, \tag{43}$$

$$I_{a_i N} = \int_{S_{N_i}} \psi_{a_i}(\mathbf{r}_i) dS_{N_i}, \tag{44}$$

$$I_{a_i e_i} = \int_{V_1} \psi_{a_i}(\mathbf{r}) \psi_{e_i}(\mathbf{r}) dV_1, \tag{45}$$

$$I_{a_i p} = \int_{S_P} \psi_{a_i}(\mathbf{r}_P) \phi_p(\mathbf{r}_P) dS_P \tag{46}$$

$$I_{e_i p} = \int_{S_P} \psi_{e_i}(\mathbf{r}_P) \phi_p(\mathbf{r}_P) dS_P, \tag{47}$$

where the index i refers to cavity 1 or 2. This formulation makes it possible to determine unknown modal pressure amplitudes for the standing waves in the cavities \bar{p}_{a_i} and the modal displacement amplitudes of the plate \bar{w}_p . Note that \bar{p}_{e_i} is a function of \bar{p}_{a_i} (Eq. (31) and Eq. (38)) and does not represent an additional variable. Combining the calculated modal amplitudes with the known rigid-wall acoustic mode shapes and the *in vacuo* structural mode shapes, the coupled system response at an arbitrary harmonic excitation can be obtained. The explicit formulation for the problem-specific cylindrical cavities and the circular plate is presented in Appendix A, including the analytically evaluated characteristic integrals from Eq. (42)-(47). The thermo-viscous losses can be implemented with the viscous damping terms [10], but the dissipation mechanisms are not covered in this paper.

Compared to the approach by Lee *et al.* [18], the formulation in Eq. (39)-(41) includes the pressure contribution from the evanescent waves, both in the pressure modal equations with the term $(\omega^2 - \omega_{a_i}^2) \sum_{e_i} I_{a_i e_i} \bar{p}_{e_i}$ and in the displacement modal equation with the term $\sum_p I_{e_1 p} \bar{p}_{e_1}$, along with the reflections of the evanescent waves. On the other hand, Lee *et al.* [18] incorporated evanescent waves only into the inertial attached neck length (Eq. (37)). Otherwise, the system of governing equations is equivalent to that of Cui and Harné [20] without considering the evanescent waves. The effect of the neck length and the evanescent waves will be further discussed in Sections 3.1 and 3.5.

3. Results and discussion

The proposed modal-interaction model was applied to the coupled system of a Helmholtz resonator and an impedance tube filled with a heavy fluid (Fig. 1). Three different variants of the elastic Helmholtz resonators, with the first mode in the frequency range 100–200 Hz, were chosen for the comparison. The designs have varying plate thickness h , neck radius R_N and tube radius R_2 , but otherwise feature the same length of the impedance tube and same geometry of the resonator cavity (Tab. 1). The resonator configurations are denoted with respect to the plate’s thickness: resonator T2, T5 and T8. Bigger tube radius was assigned to the resonator T2 to avoid frequency shift of the resonator mode due to the small tube-to-neck radius ratio. The acoustic properties of the heavy fluid and the mechanical properties of the elastic plate are presented in Tab. 2. In order to obtain the response of the system, the effective neck length must be calculated first.

Table 1: Resonator configurations and corresponding geometric parameters.

	h [mm]	R_N [mm]	L_N [mm]	R_1 [mm]	L_1 [mm]	R_2 [mm]	L_2 [mm]
Resonator T2	2	24				100	
Resonator T5	5	4	22	80.5	22	39.5	3000
Resonator T8	8	2				39.5	

Table 2: Material properties of the elastic plate and the acoustic fluid.

	Plate	Fluid
$\rho_P =$	7850 kg/m ³	$\rho =$ 916 kg/m ³
$E =$	210 GPa	$c =$ 1380 m/s
$\nu =$	0.3	

3.1. Effective neck length

The evanescent waves formulation makes it possible to determine the length correction for the neck between cavities with an arbitrary geometry. Following

Eq. 37, the current model produces the same results as Lee *et al.* [18] due to the cancellation of the decay-rate parameter $C_{n_i s_i}(z_i)$, meaning that the reflections of the evanescent waves do not have an effect on the inertial attached length of the neck. Furthermore, considering the shape of the cross-modes in Eq. (23), it is clear that only the axisymmetric modes contribute to the inertial attached neck length in the case of the concentric cavities and the neck.

The convergence of the inertial attached neck length in relation to the number of used cross-modes n_i, s_i is presented in Fig. 4. It is clear that the number of cross-modes participating in the inertial attached length increases with the decreasing diameter of the neck. In contrast, the inertial attached neck length increases simultaneously with the neck diameter.

Approximations from the literature, $\Delta L = 1.7 R_N$ according to Kinsler *et al.* [21] and $\Delta L = \frac{1}{3}\sqrt{S_N}$ according to Fahy [1], are also shown in Fig. 4, although they are independent of the number of modes. Considerable discrepancies can be observed between the methods, with Kinsler’s being more appropriate for a small neck-to-cavity cross-section ratio and the opposite for Fahy’s. Kinsler’s approximation was used in the studies of Ahn *et al.* [19] and Cui *et al.* [20].

3.2. Model validation

The modal-interaction method was validated based on the FEA simulations conducted using Ansys software. Simulations were performed with the direct two-way coupling between the elastic plate and the acoustic fluid. Therefore, the fluid-structure interaction was implemented with the coupling terms in the element matrix, which results in an unsymmetric matrix [31]. Thermo-viscous losses in the fluid were neglected, both the intrinsic viscosity damping and the dissipation in the boundary layer [32], as the proposed model does not account for these absorption mechanisms. A fixed support was placed on the edge of the plate for clamped boundary condition.

Mesh was composed of quadratic and predominantly hexahedral elements. The cavities and the neck were modeled with 3D acoustic elements FLUID220. The plate area was meshed with shell elements SHELL281, governed by the first-order shear-deformation theory, also referred to as the Mindlin–Reissner shell theory. The required number of elements to achieve the converged solution is presented in Tab. 3 for each resonator configuration.

Table 3: Number of elements in the FEA model.

	Plate	Neck	Cavity 1	Cavity 2
Resonator T2	1025	2744	8200	123667
Resonator T5	8376	9768	309912	189275
Resonator T8	8316	10498	482328	130424

The current implementation of the modal-interaction model is derived from the differential equation for thin plates guided by the Kirchhoff-Love theory. The extent of the modes participating in Eq. 39-41 was chosen based on the

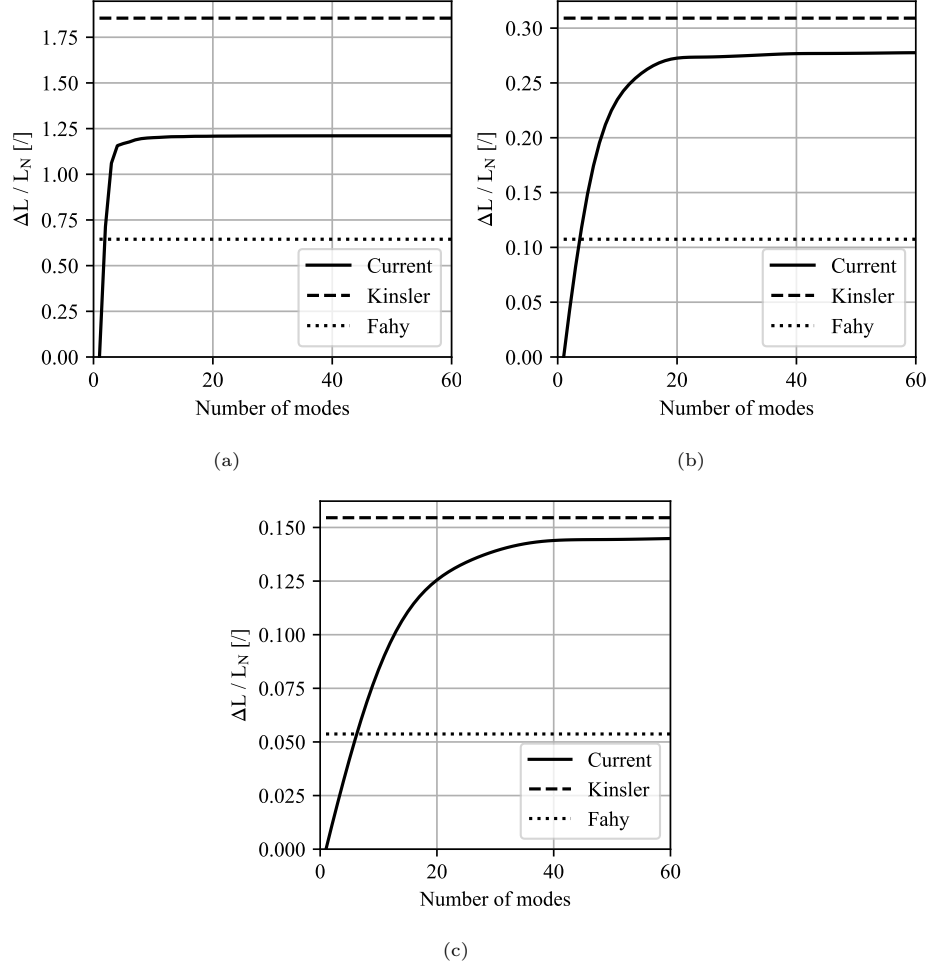


Figure 4: Non-dimensional inertial attached neck length $\frac{\Delta L}{L_N}$ obtained with different methods, Evanescent: calculated with Eq. (37) at $\omega = 100$ Hz, Kinsler: $\Delta L = 1.7 R_N$ [21], Fahy: $\Delta L = \frac{1}{3}\sqrt{S_N}$ [1]; a) Resonator T2, b) Resonator T5, c) Resonator T8.

plane-wave excitation in the frequency range 100–2100 Hz. Using the notations from Appendix A, the solution converged when using the mode orders:

$$\begin{aligned} n_1 = 0, \quad s_1 \in [0, 3], \quad l_1 \in [0, 3], \\ n_2 = 0, \quad s_2 \in [0, 3], \quad l_2 \in [0, 150], \end{aligned}$$

for the cavity mode shapes $\psi_{n_i s_i l_i}(r, \theta, z)$, and:

$$n = 0, \quad m \in [0, 3],$$

for the plate mode shapes $\phi_{nm}(r, \theta)$. These sets incorporate modes with a natural frequency as high as 65583 Hz for cavity 1, 39064 Hz for cavity 2 and

6768 Hz for the plate. The higher order of the longitudinal acoustic modes is used to take into account the strong coupling between the heavy fluid and the plate. These higher-order modes, labeled non-resonant acoustic modes, coincide spatially with the plate modes of lower orders and induce added stiffness and mass to the plate [30]. The axisymmetric geometry makes it possible to reduce the extent of the problem by using the same indices for the standing and evanescent waves due to the orthogonality of the cross-modes, i.e., the coupling integral $I_{a_1 e_1}$ having a non-zero solution only in that case.

The proposed model and the FEA model were excited with the surface normal velocity $\bar{q}_2 = 10 \text{ s}^{-1}$ applied to the entrance surface of the impedance tube ($z = 0$ in Fig. 2) and the displacement at the center of the plate was observed. The results in Fig. 5 show good agreement between the methods over a wide frequency range for resonators with a smaller neck cross-section (T5 and T8). For the case of resonator T2 with the widest neck, the coinciding results are limited to the frequencies below 1500 Hz. More accurate results in the higher frequency range would be achieved by using the general Dowell *et al.* [16] theory with inner coupling of the acoustic cavities through a virtual zero mass and stiffness membrane, since the neck dynamics can no longer be considered to be the equivalent of a lumped mass.

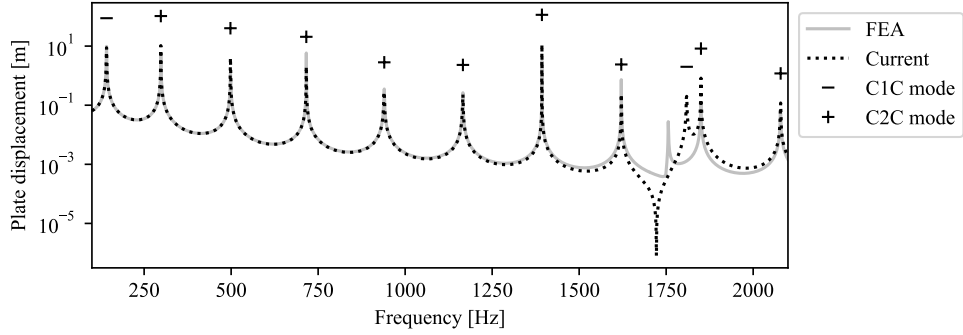
3.3. Coupled modes

Peaks in Fig. 5 represent the modes of the coupled system of the impedance tube and different resonator configurations. Based on the amount of energy contained in the acoustic cavities, the spectrum peaks are marked as cavity-1-controlled modes, if most of the energy is stored in the cavity-1 sound field, or marked as cavity-2-controlled modes, when most of the energy is located in the cavity-2 sound field. The considerable length of the impedance tube causes a higher density of cavity-2-controlled modes in the low-frequency range. Due to the strong coupling between cavity 1 and the plate, one cannot distinguish between the cavity-1-controlled mode and the plate-controlled mode, as opposed to the distinct separation in the weakly coupled systems [33]. Therefore, the cavity-1 dominant modes in Fig. 5 represent the coupled structural-acoustic modes of the elastic Helmholtz resonator.

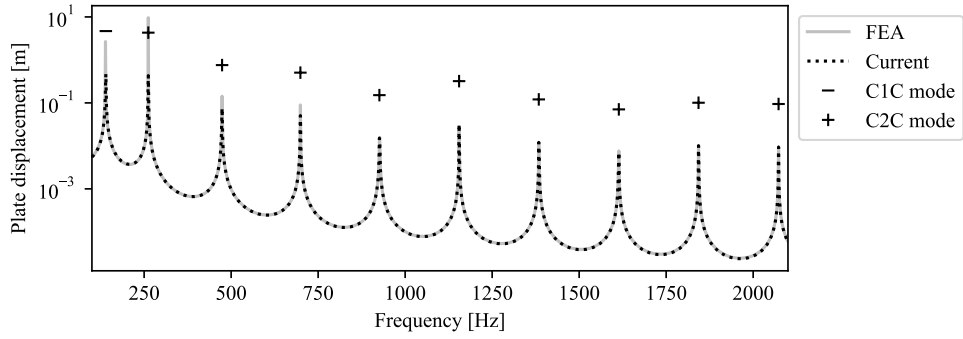
Frequencies of the first five coupled modes in Fig. 5a are summarized in Tab. 4. Frequencies of the uncoupled modes of the plate and cavities, obtained with Eq. (70) and (65) (excluding the zero-frequency static pressure mode), are also presented for comparison. The frequency of the cavity-1-controlled coupled mode differs greatly from the natural frequencies of the clamped elastic plate and the rigid-wall cavity 1 due to the strong fluid-structure interaction. On the other hand, cavity-2-controlled modes are more comparable to the rigid-wall modes of the cavity 2, but still influenced by the coupling between the cavities through the neck.

3.4. Mindlin-Reissner plate

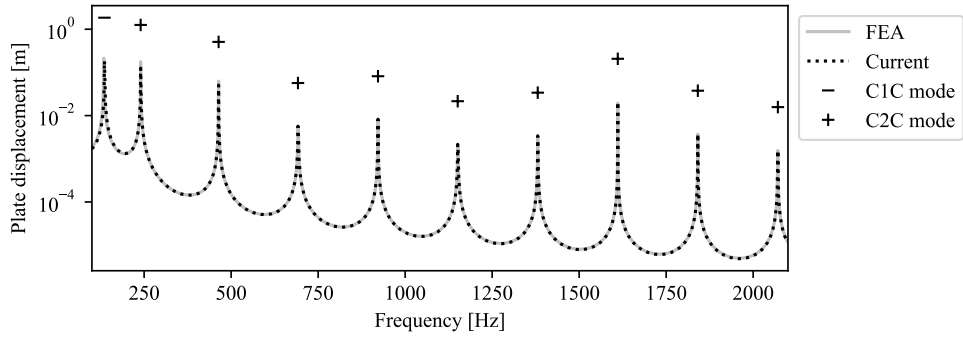
Focusing on the first coupled mode (cavity-1-controlled mode) in Fig. 5, an accurate plate displacement can be observed for the resonator T2 (Fig. 6). On



(a)



(b)



(c)

Figure 5: Displacement amplitude at the center of the plate, FEA: FEA model, Current: proposed modal-interaction model, C1C mode: cavity-1-controlled mode, C2C mode: cavity-2-controlled mode; a) Resonator T2, b) Resonator T5, c) Resonator T8.

the other hand, the moderately thick plates in the resonators T5 and T8 cause discrepancies between the FEA results and the proposed model. While the first analysis method employs the Mindlin–Reissner plate theory, the latter is

Table 4: Natural frequencies of the coupled system with resonator T2 (C1C mode: cavity-1-controlled mode, C2C mode: cavity-2-controlled mode) and natural frequencies of the uncoupled plate and cavities.

Mode	Frequency [Hz]			
	Coupled	Plate	Cavity 1	Cavity 2
1	141.8 (C1C)	785.4	5023.4	230
2	297.9 (C2C)	1634.5	8333.1	460
3	498.1 (C2C)	2681.4	10454.3	690
4	715.9 (C2C)	3057.7	11462.4	920
5	939.5 (C2C)	3923.3	14508.3	1150

based on the Kirchhoff-Love plate theory, which neglects the shear deformations throughout the plate thickness. Therefore, the current model overestimates the plate stiffness and shifts the cavity-1-controlled modes to the higher frequencies.

As presented in Fig. 6, more accurate results can be achieved by using the Mindlin-Reissner formulation to obtain the mode shapes $\psi_{n_i s_i l_i}(r, \theta, z)$ for the thick plates (see Appendix A.3). In the interest of limiting the complexity of the system, the Kirchhoff-Love-based formulation in Eq. 39-41 is still used to calculate the modal pressure and displacement amplitudes. This approach will be used in subsequent analyses in the section.

3.5. Effect of evanescent waves

The main difference between the present model and the formulations of Lee *et al.* [17, 18] and Cui *et al.* [20] is the implementation of the evanescent waves. The study by Cui *et al.* [20] does not explicitly acknowledge the effect of evanescent waves on the pressure field, but an approximate inertial attached length of the neck was taken into account. While Lee *et al.* [17, 18] determined the inertial attached neck length from the distribution of the evanescent waves, the derived governing equations were equivalent to those of Cui *et al.* [20]. Finally, the proposed approach extends the formulation of Lee *et al.* [18] to include the reflected evanescent waves in short cavities and obtains a system of governing equations with terms for the corresponding pressure modes.

The relevance of the evanescent waves is presented in Fig. 7. All the approaches are modified to include the Mindlin-Reissner mode shapes of the plate. Since the model by Cui *et al.* [20] is limited to a resonator in the free field, it was first expanded to include the acoustic fluid in the impedance tube. Regarding the results in Fig. 7, the substantial discrepancy by Cui *et al.* [20] for resonator T2 is in accordance with the large deviation of the calculated effective neck length using the approximate formula [21] (Fig. 4). Note the expanded frequency range in Fig. 7a. Analogously, the results are more comparable for the thicker plates in resonators T5 and T8. The errors resulting from the alternative formulations are the smallest in the case of the resonator T8, indicating that the effect of the evanescent waves is decreasing with the reduction of the neck diameter. Furthermore, the influence of the evanescent waves decreases in the higher frequency range due to shorter wavelength, as shown with smaller

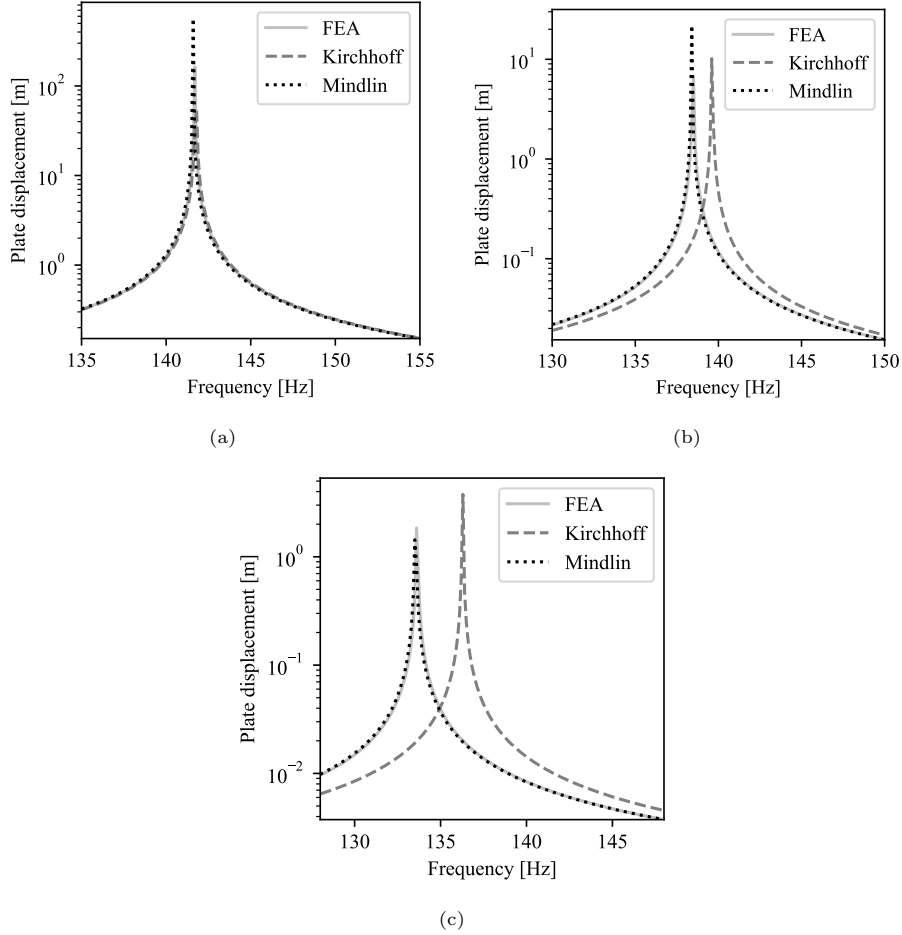


Figure 6: Displacement amplitude at the center of the plate for the first coupled mode, FEA: FEA with the Mindlin–Reissner plate theory, Kirchhoff: proposed model with the Kirchhoff–Love plate theory, Mindlin: proposed model with the Mindlin–Reissner mode shapes and the Kirchhoff–Love modal amplitudes; a) Resonator T2, b) Resonator T5, c) Resonator T8.

peaks’ deviations for higher modes in Fig. 8. In general, previous methods predict lower natural frequencies of the coupled modes compared to the proposed model and the FEA results.

The influence of the evanescent waves on the pressure distribution is even more obvious when observing a system of coupled cavities with acoustically rigid walls, as shown in Fig. 9. In comparison to the initial coupled structural–acoustic system in Fig. 2, the elastic plate is now absent and only the acoustic coupling between two cavities connected through a neck is present. First, the eigenvalue problem is derived by eliminating the structural terms and the excitation sources from the governing equations (see Appendix A.4). Then, the

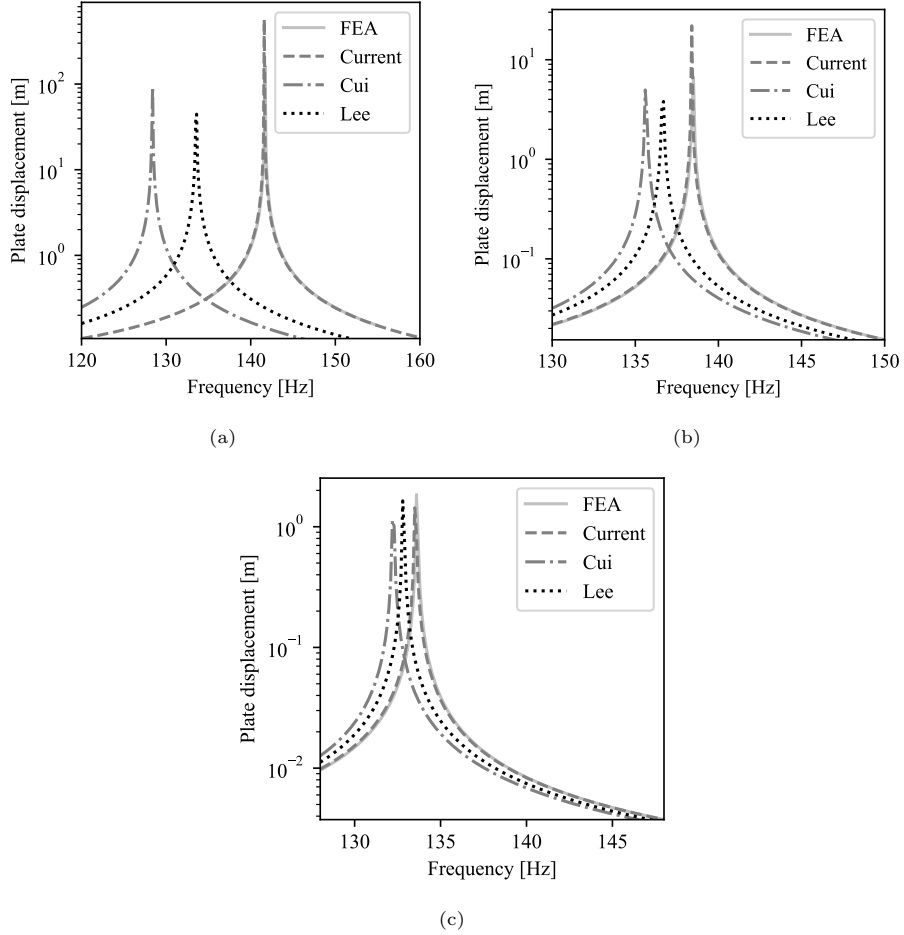


Figure 7: Displacement amplitude at the center of the plate for the first coupled mode, FEA: FEA model, Current: proposed model, Cui: model by Cui and Harne [20], Lee: model by Lee *et al.* [18]; a) Resonator T2, b) Resonator T5, c) Resonator T8.

system can be solved for the eigenvalues and eigenvectors, although an iterative method must be employed due to the frequency dependence of the neck-length correction. With the resulting eigenvalues and eigenvectors we obtain the natural frequencies of the coupled acoustic modes and the normalized pressure mode shapes.

The eigenvalue analysis was conducted on the resonator T2 with the greatest inertial attached neck length and the impedance tube with reduced length $L_2 = 150$ mm and radius $R_2 = 39.5$ mm, for the purposes of an easier representation of the results. The calculated natural frequencies of the first coupled mode are listed in Tab. 5 and the corresponding pressure mode shapes are shown in Fig. 10. The frequency deviations from the FEA results are in accordance

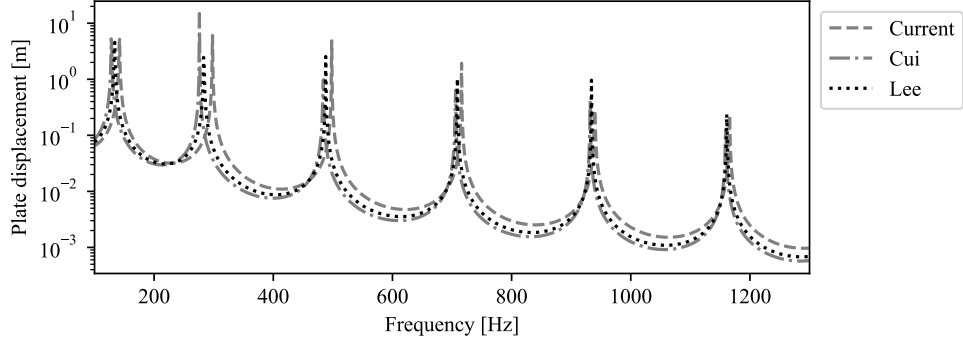


Figure 8: Displacement amplitude at the center of the plate for resonator T2, Current: proposed model, Cui: model by Cui and Harne [20], Lee: model by Lee *et al.* [18].

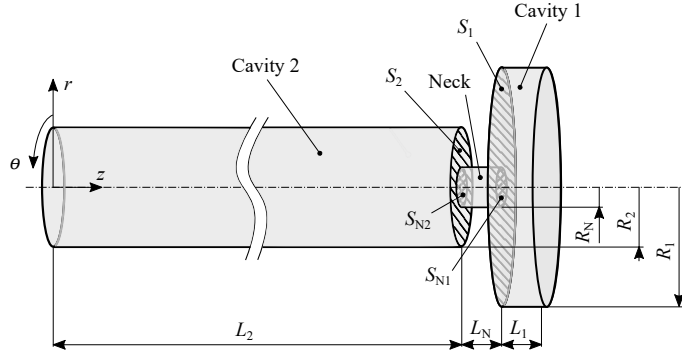


Figure 9: Acoustic system with two cavities coupled through a neck.

with the previous findings. Fig. 10 presents the mid-plane pressure solution in the cavities, while the pressure field inside the neck is masked for analytical methods. Contour plots of the pressure distribution confirm that the proposed method is the most accurate with respect to the FEA results.

Table 5: Natural frequency of the first coupled acoustic mode obtained with different methods.

Method	Frequency [Hz]
FEA	2204.9
Proposed model	2195.5
Cui and Harne [20]	1755.0
Lee <i>et al.</i> [18]	1980.9

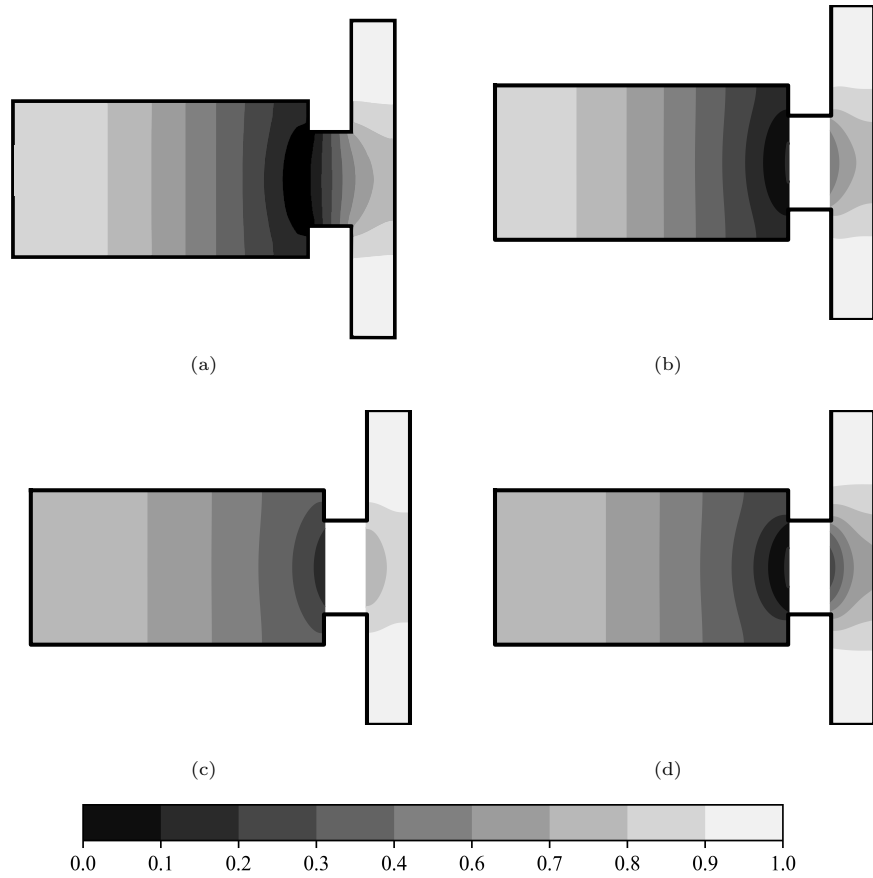


Figure 10: Normalized pressure distribution of the first coupled acoustic mode; a) FEA model, b) Proposed model, c) Cui and Harne [20], d) Lee *et al.* [18].

4. Conclusion

The improved analytical model of a structural–acoustic system with two cavities coupled through a neck and the fluid–structure interaction between a heavy fluid and a plate was developed in this paper. A conventional modal–interaction approach was employed to derive the governing equations for the cavities and the plate, whereas the neck dynamics were represented with a lumped–parameter model. While other available methods implement the effect of the evanescent waves only implicitly with the inertial attached length of the neck, our method achieves better accuracy with the additional terms of evanescent pressure modes in the governing equations. Furthermore, the definition of the evanescent pressure field was redefined to allow reflections of the evanescent waves from the cavity walls, thus overcoming the restrictions of other models that can only be used on cavities with a specific geometry. The proposed formulation also

improves the performance of the model for moderately thick plates with the implementation of the Mindlin–Reissner plate theory.

The proposed model was applied to the vibro-acoustic system of an elastic Helmholtz resonator coupled to an impedance tube, where the acoustic cavities were filled with a liquid medium. Three different configurations of the resonator were utilized, with varying plate thickness, neck radius and impedance tube radius. Firstly, the influence of the resonator’s geometry on the effective neck length was studied. Discrepancies between the inertial attached neck length calculated with the approximate formulas from the literature and the inertial attached neck length obtained by the formulation with evanescent waves highlighted the importance of adjusting the neck length with respect to the problem-specific geometry.

The new method was validated on the basis of a comparison with the FEA results. Good agreement was observed for the resonator with a large neck diameter, up to a frequency of 1500 Hz. This also confirms that the appropriate number of structural and acoustic modes was used to account for the strong coupling mechanism between the heavy fluid and the plate. Closer inspection of the low-frequency response spectrum revealed deviations for the resonators with thicker plates, due to the neglected shear deformations in the Kirchhoff-Love plate theory. With the implementation of the Mindlin–Reissner plate theory to obtain the mode shapes for moderately thick plates, improved accuracy of the model was achieved.

Finally, a comprehensive study of the effect of evanescent waves on the pressure distribution was performed. A comparison of the methods with different approaches to the implementation of the evanescent pressure field showed that the systematic incorporation in the current model is crucial for accurate results. The eigenvalue problem analysis conducted on the isolated acoustic part of the system confirmed that the proposed model produces equivalent results to the FEA simulation even around the geometric discontinuities, while discrepancies were observed with the other methods.

All things considered, the presented model is the preferred analytical method for the analysis of an elastic Helmholtz resonator coupled to an impedance tube through a heavy fluid in the low- to mid-frequency range. Due to the included strong fluid-structure interaction and the formulation of the evanescent waves, the developed model can be used on systems with heavy fluids and acoustic cavities having arbitrary geometries.

Appendix A

Following notations will be used in analytical evaluation of the characteristic integrals:

$$\kappa_{n_i}^\theta = \begin{cases} 2\pi & n = 0 \\ \pi & n > 0 \end{cases}, \quad (48)$$

$$\kappa_{l_i}^z = \begin{cases} L_i & l = 0 \\ \frac{L_i}{2} & l > 0 \end{cases}, \quad (49)$$

$$E_{n_i s_i} = \begin{cases} \pi R_N^2 & n_i = 0, \beta_{n_i s_i} = 0 \\ \frac{2\pi R_i R_N}{\beta_{n_i s_i}} J_1(\beta_{n_i s_i} \frac{r}{R_i}) & n_i = 0, \beta_{n_i s_i} \neq 0 \\ 0 & n_i \neq 0 \end{cases}, \quad (50)$$

$$H_{n_i s_i}^\beta = \frac{R_i^2}{2} \left(1 - \frac{n_i^2}{\beta_{n_i s_i}^2}\right) J_{n_i}^2(\beta_{n_i s_i}), \quad (51)$$

$$H_{inm}^\delta = \frac{R_1^2}{2} \left[(J'_n(\delta_{inm}))^2 + \left(1 - \frac{n^2}{\delta_{inm}^2}\right) J_n^2(\delta_{inm}) \right], \quad (52)$$

$$G_{nm}^\delta = \frac{R_1^2}{\delta_{1nm}^2 - \delta_{2nm}^2} [\delta_{2nm} J_n(\delta_{1nm}) J'_n(\delta_{2nm}) - \delta_{1nm} J_n(\delta_{2nm}) J'_n(\delta_{1nm})], \quad (53)$$

$$F_{inms} = \frac{\delta_{inm} R_1^2}{\beta_{ns}^2 - \delta_{inm}^2} J_n(\beta_{ns}) J'_n(\delta_{inm}), \quad (54)$$

$$F_{nms}^J = \frac{\lambda_{nm} R_1^2}{\beta_{ns}^2 - \lambda_{nm}^2} J_n(\beta_{ns}) J'_n(\lambda_{nm}), \quad (55)$$

$$F_{nms}^I = \frac{\lambda_{nm} R_1^2}{\beta_{ns}^2 + \lambda_{nm}^2} J_n(\beta_{ns}) I'_n(\lambda_{nm}). \quad (56)$$

A.1 Acoustic cavity

Mode shapes of the standing and the evanescent wave in the acoustic cavities and corresponding integrals are defined as:

$$\psi_{a_1}(\mathbf{r}) = \psi_{n_1 s_1 l_1}(r, \theta, z) = J_{n_1} \left(\beta_{n_1 s_1} \frac{r}{R_1} \right) \cos(n_1 \theta) \cos \left(l_1 \pi \frac{z - (L_2 + L_N)}{L_1} \right), \quad (57)$$

$$\psi_{a_2}(\mathbf{r}) = \psi_{n_2 s_2 l_2}(r, \theta, z) = J_{n_2} \left(\beta_{n_2 s_2} \frac{r}{R_2} \right) \cos(n_2 \theta) \cos \left(l_2 \pi \frac{z}{L_2} \right), \quad (58)$$

$$\phi_{n_i s_i}(r, \theta) = J_{n_i} \left(\beta_{n_i s_i} \frac{r}{R_i} \right) \cos(n_i \theta), \quad (59)$$

$$\mu_{a_i} = \kappa_{n_i}^\theta \kappa_{l_i}^z H_{n_i s_i}^\beta, \quad (60)$$

$$I_{a_1 N} = E_{n_1 s_1}, \quad (61)$$

$$I_{a_2 N} = (-1)^{l_2} E_{n_2 s_2}, \quad (62)$$

$$I_{a_1 e_1} = \kappa_{n_1}^\theta H_{n_1 s_1} \frac{\alpha_{n_1 s_1} L_1^2 (1 - e^{-2\alpha_{n_1 s_1} L_1 M})}{\alpha_{n_1 s_1}^2 L_1^2 + \pi l_1^2}, \quad (63)$$

$$I_{a_2 e_2} = \kappa_{n_2}^\theta H_{n_2 s_2} \frac{(-1)^{l_2+1} \alpha_{n_2 s_2} L_2^2 e^{-2\alpha_{n_2 s_2} L_2 M} + (-1)^{l_2} \alpha_{n_2 s_2} L_2^2}{\alpha_{n_2 s_2} L_2^2 + \pi^2 l_2^2}, \quad (64)$$

where n refers to circumferential, s to radial and l to axial mode order. Natural frequencies of the acoustic cavity i are calculated with the following equation:

$$\omega_{n_i s_i l_i} = c \sqrt{\left(\frac{\beta_{n_1 s_1}}{R_i}\right)^2 + \left(\frac{l_i \pi}{L_i}\right)^2}. \quad (65)$$

A.2 Kirchhoff-Love plate theory

In the case of a thin plate with eigenvalues λ_{nm} the following equations apply:

$$\phi_p(\mathbf{r}_P) = \phi_{nm}(r, \theta) = J_n\left(\lambda_{nm} \frac{r}{R_1}\right) - \frac{J_n(\lambda_{nm})}{I_n(\lambda_{nm})} I_n\left(\lambda_{nm} \frac{r}{R_1}\right), \quad (66)$$

$$\mu_p = \kappa_n^\theta R_1^2 J_n(\lambda_{nm}), \quad (67)$$

$$I_{a_i p} = \kappa_n^\theta \left[F_{nms}^J - \frac{J_n(\lambda_{nm})}{I_n(\lambda_{nm})} F_{nms}^I \right], \quad (68)$$

$$I_{e_i p} = \kappa_n^\theta \left[F_{nms}^J - \frac{J_n(\lambda_{nm})}{I_n(\lambda_{nm})} F_{nms}^I \right] \frac{1 - e^{-2\alpha_{n_1 s_1} L_1 M}}{\sinh(\alpha_{n_1 s_1} L_1)}. \quad (69)$$

where n and m represent the circumferential and radial mode order. Natural frequencies of the plate are obtained with equation:

$$\omega_{nm} = \frac{\lambda_{nm}^2}{R_1^2} \sqrt{\frac{D}{\rho_p h}}. \quad (70)$$

A.3 Mindlin-Reissner plate theory

For thick plates the formulation is adjusted as follows:

$$\phi_p(\mathbf{r}_P) = \phi_{nm}(r, \theta) = J_n\left(\delta_{1nm} \frac{r}{R_1}\right) - \frac{J_n(\delta_{1nm})}{J_n(\delta_{2nm})} J_n\left(\delta_{2nm} \frac{r}{R_1}\right), \quad (71)$$

$$\mu_p = \kappa_n^\theta \left[H_{1nm}^\delta - 2 \frac{J_n(\delta_{1nm})}{J_n(\delta_{2nm})} G_{nm}^\delta + \frac{J_n^2(\delta_{1nm})}{J_n^2(\delta_{2nm})} H_{2nm}^\delta \right], \quad (72)$$

$$I_{a_i p} = \kappa_n^\theta \left[F_{1nms} - \frac{J_n(\delta_{1nm})}{J_n(\delta_{2nm})} F_{2nms} \right], \quad (73)$$

$$I_{e_i p} = \kappa_n^\theta \left[F_{1nms} - \frac{J_n(\delta_{1nm})}{J_n(\delta_{2nm})} F_{2nms} \right] \frac{1 - e^{-2\alpha_{n_1 s_1} L_1 M}}{\sinh(\alpha_{n_1 s_1} L_1)}. \quad (74)$$

where δ_{1nm} and δ_{2nm} are dimensionless parameters affiliated with eigenvalue λ_{nm} [34].

A.4 Eigenvalue problem

Eigenvalues and eigenvectors of the coupled cavities 1 and 2 are obtained by solving the eigenvalue problem:

$$\mu_{a_1} (\omega^2 - \omega_{a_1}^2) \bar{p}_{a_1} + (\omega^2 - \omega_{a_1}^2) \sum_{e_1} I_{a_1 e_1} \bar{p}_{e_1} -$$

$$-\frac{c^2}{S_N L'_N} I_{a_1 N} \left(\sum_{a_1} I_{a_1 N} \bar{p}_{a_1} - \sum_{a_2} I_{a_2 N} \bar{p}_{a_2} \right) = 0, \quad (75)$$

$$\begin{aligned} & \mu_{a_2} (\omega^2 - \omega_{a_2}^2) \bar{p}_{a_2} + (\omega^2 - \omega_{a_2}^2) \sum_{e_2} I_{a_2 e_2} \bar{p}_{e_2} + \\ & + \frac{c^2}{S_N L'_N} I_{a_2 N} \left(\sum_{a_1} I_{a_1 N} \bar{p}_{a_1} - \sum_{a_2} I_{a_2 N} \bar{p}_{a_2} \right) = 0. \end{aligned} \quad (76)$$

References

- [1] F. Fahy, Foundations of engineering acoustics, Academic Press, Oxford, 2001.
- [2] D. M. Photiadis, The effect of wall elasticity on the properties of a helmholtz resonator, *J. Acoust. Soc. Am.* 90 (1991) 1188–1190. doi:10.1121/1.402026.
- [3] A. N. Noris, Elastic helmholtz resonators, *J. Acoust. Soc. Am.* 93 (1993) 617–630. doi:10.1121/1.405481.
- [4] U. Farooq, S. S. Nudehi, A nonlinear acoustic resonator, *ASME* 1 (2007) 2015–2022. doi:10.1115/DETC2007-34700.
- [5] S. S. Nudehi, U. Farooq, E. Motato, Perturbation analysis of a nonlinear resonator, *ASME* 8 (2009) 1–8. doi:10.1115/1.4005998.
- [6] S. S. Nudehi, G. S. Duncan, U. Farooq, Modeling and experimental investigation of a helmholtz resonator with a flexible plate, *J. Vib. Acoust.* 135 (2013) 1–6. doi:10.1115/1.4023810.
- [7] M. H. Kurdi, G. S. Duncan, S. S. Nudehi, Optimal design of a helmholtz resonator with flexible end plate, *J. Vib. Acoust.* 136 (2014) 1–8. doi:10.1115/1.4026849.
- [8] Z.-F. Wang, Y.-M. Hu, S.-D. Xiong, H. Luo, Z. Meng, M. Ni, Influence of cavity wall elasticity on resonant frequency of small underwater cylindrical helmholtz resonator, *Acta Physica Sinica* 58 (2009) 2507–2512.
- [9] G. Hu, L. Tang, X. Cui, On the modelling of membrane-coupled helmholtz resonator and its application in acoustic metamaterial system, *Mechanical Systems and Signal Processing* 132 (2019) 595–608. doi:10.1016/j.ymsp.2019.07.017.
- [10] F. Fahy, P. Gardonio, Sound and structural vibration: Radiation, transmission and response, Academic Press, Oxford, 2007.

- [11] F. J. Fahy, Vibration of containing structures by sound in the contained fluid, *Journal of Sound and Vibration* 10 (1969) 490–512. doi:10.1016/0022-460X(69)90228-4.
- [12] F. J. Fahy, Response of a cylinder to random sound in the contained fluid, *Journal of Sound and Vibration* 13 (1970) 171–194. doi:10.1016/S0022-460X(70)81172-5.
- [13] J. T. Du, W. L. Li, Z. G. Liu, H. A. Xu, Z. L. Ji, Acoustic analysis of a rectangular cavity with general impedance boundary conditions, *J. Acoust. Soc. Am.* 130 (2011) 807–817. doi:10.1121/1.3605534.
- [14] J. T. Du, W. L. Li, H. A. Xu, Z. G. Liu, Vibro-acoustic analysis of a rectangular cavity bounded by a flexible panel with elastically restrained edges, *J. Acoust. Soc. Am.* 131 (2011) 2799–2810. doi:10.1121/1.3693652.
- [15] M. Pirnat, G. Čepon, M. Boltežar, Structural–acoustic model of a rectangular plate–cavity system with an attached distributed mass and internal sound source: Theory and experiment, *Journal of Sound and Vibration* 333 (2014) 2003–2018. doi:10.1016/j.jsv.2013.11.044.
- [16] E. H. Dowell, G. F. Gorman III, D. A. Smith, Acoustoelasticity: General theory, acoustic natural modes and forced response to sinusoidal excitation, including comparisons with experiment, *Journal of Sound and Vibration* 52 (1977) 519–542. doi:10.1016/0022-460X(77)90368-6.
- [17] J. W. Lee, J. M. Lee, S. H. Kim, Acoustical analysis of multiple cavities connected by necks in series with a consideration of evanescent waves, *Journal of Sound and Vibration* 273 (2004) 515–542. doi:10.1016/S0022-460X(03)00508-X.
- [18] J. W. Lee, J. M. Lee, An improved mode superposition method applicable to a coupled structural–acoustic system with a multiple cavity, *Journal of Sound and Vibration* 301 (2007) 821–845. doi:10.1016/j.jsv.2006.10.025.
- [19] C.-G. Ahn, H. G. Cho, J. M. Lee, Structural-acoustic coupling analysis of two cavities connected by boundary structures and small holes, *J. Vib. Acoust.* 127 (2005) 566–574. doi:10.1115/1.2110880.
- [20] S. Cui, R. L. Harne, Soft materials with broadband and near-total absorption of sound, *Phys. Rev. Applied* 12 (2019) 1–12. doi:10.1103/PhysRevApplied.12.064059.
- [21] L. E. Kinsler, A. R. Frey, A. B. Coppens, J. V. Sanders, *Fundamentals of acoustics*, John Wiley & Sons, Inc., New York, 1999.
- [22] F. J. Fahy, C. Schofield, A note on the interaction between a helmholtz resonator and an acoustic mode of an enclosure, *Journal of Sound and Vibration* 72 (1980) 365–378. doi:10.1016/0022-460X(80)90383-1.

- [23] A. Cummings, The effects of a resonator array on the sound field in a cavity, *Journal of Sound and Vibration* 154 (1992) 25–44. doi:10.1016/0022-460X(92)90402-J.
- [24] D. Li, L. Cheng, Acoustically coupled model of an enclosure and a helmholtz resonator array, *Journal of Sound and Vibration* 305 (2007) 272–288. doi:10.1016/j.jsv.2007.04.009.
- [25] Z. Wang, Y. Choy, Acoustical coupling and radiation control of open cavity using an array of helmholtz resonators, *Mechanical Systems and Signal Processing* 130 (2019) 632–648. doi:10.1016/j.ymsp.2019.05.037.
- [26] S. Cui, R. L. Harne, Acoustic-structure interaction in an adaptive helmholtz resonator by compliance and constraint, *Journal of Vibration and Acoustics* 142 (2020) 617–630. doi:10.1115/1.4045456.
- [27] S. M. Kim, M. J. Brennan, A compact matrix formulation using the impedance and mobility approach for the analysis of structural-acoustic systems, *Journal of Sound and Vibration* 223 (1999) 97–113. doi:10.1006/jsvi.1998.2096.
- [28] J.-M. David, M. Menelle, Validation of a medium-frequency computational method for the coupling between a plate and a water-filled cavity, *Journal of Sound and Vibration* 265 (2003) 841–861. doi:10.1016/S0022-460X(02)01529-8.
- [29] J.-M. David, M. Menelle, Validation of a modal method by use of an appropriate static potential for a plate coupled to a water-filled cavity, *Journal of Sound and Vibration* 301 (2007) 739–759. doi:10.1016/j.jsv.2006.10.033.
- [30] L. Maxit, Analysis of the modal energy distribution of an excited vibrating panel coupled with a heavy fluid cavity by a dual modal formulation, *Journal of Sound and Vibration* 332 (2013) 6703–6724. doi:10.1016/j.jsv.2013.07.020.
- [31] C. Q. Howard, B. S. Cazzolato, *Acoustic analyses using Matlab and Ansys*, CRC Press, Boca Raton, 2015.
- [32] R. Bossart, N. Joly, M. Bruneau, Hybrid numerical and analytical solutions for acoustic boundary problems in thermo-viscous fluids, *Journal of Sound and Vibration* 263 (2003) 69–84. doi:10.1016/j.jsv.2013.11.044.
- [33] J. Pan, D. A. Bies, The effect of fluid–structural coupling on sound waves in an enclosure - theoretical part, *J. Acoust. Soc. Am.* 87 (1990) 691–707. doi:10.1121/1.398939.
- [34] K. M. Liew, C. M. Wang, Y. Xiang, S. Kitipornchai, *Vibration of Mindlin plates: Programming the p-version Ritz method*, Elsevier, Oxford, 1998.